ISSN: 2538-2152; ECOPERSIA 2025;13(4): 341-361.

Advanced Flood Hazard Assessment using Frequency Storm, HEC-RAS 2D, and AIDR in the RAS Mapper Environment for the Tireh Dorud River in Iran

ARTICLEINFO

Article Type
Original Research

Authors
Zahra Naserian Asl, *Ph.D. Student*[1]
Hoda Ghasemieh, *Ph.D.*[2*]

How to cite this article
Naserian Asl Z., Ghasemieh H. Advanced Flood Hazard Assessment using Frequency Storm, HEC-RAS 2D, and AIDR in the RAS Mapper Environment for the Tireh Dorud River in Iran. ECOPERSIA 2025;13(3): 323-340.

DOI:
10.48311/ECOPERSIA.13.4.341

[1] Former Ph.D. Student, Watershed Management Sciences and Engineering, Department of Nature Engineering, Faculty of Natural Resources and Earth Sciences, University of Kashan, Kashan, Iran.
[2]Associate Professor, Watershed Management Sciences and Engineering, Department of Nature Engineering, Faculty of Natural Resources and Earth Sciences, University of Kashan, Kashan, Iran.

**** Correspondence***
Address: Associate Professor, Department of Nature Engineering, Faculty of Natural Resources and Earth Sciences, University of Kashan, Kashan, Iran
Tel: +989132613779
Email: h.ghasemieh@kashanu.ac.ir

Article History
Received: July 2, 2025
Accepted: August 28, 2025
Published: September 3, 2025

ABSTRACT

Aims: Among natural disasters, flooding is recognized as a particularly destructive phenomenon that is increasingly occurring, posing a significant threat to urban infrastructure and surrounding land-uses. As a result, assessing flood characteristics, such as depth, velocity, and the extent of inundation, across different return periods is essential. This research aimed to develop and analyze the flood hazard map for Dorud City using the two-dimensional HEC-RAS model within the RAS Mapper environment.

Materials & Methods: Initially, flood hydrographs for return periods of 2, 5, 10, 20, 50, 100, 200, and 500 years were predicted using the HEC-HMS hydrological model and the Frequency Storm methodology. These hydrographs were input into the two-dimensional HEC-RAS hydraulic model for flood hazard mapping and analysis. Geometric data (perimeters and break lines) and upstream/downstream boundary conditions were outlined in RAS Mapper using a 12.5-meter resolution Digital Elevation Model (DEM). Flood depth and velocity maps were subsequently generated for the specified return periods. Finally, flood hazard maps were created using the Australian Institute for Disaster Resilience (AIDR) method within RAS Mapper, utilizing the depth and velocity maps produced.

Findings: The results show that the flood inundation areas for the 50-, 100-, 200-, and 500-year return periods are 9.587, 9.685, 9.708, and 9.761 km^2, respectively. A significant portion of the flood-prone area is situated within the high to very high hazard zones.

Conclusion: Furthermore, the AIDR analysis indicates that these areas are unsafe for all buildings, vehicles, and individuals, highlighting the urgent need to implement flood control measures to mitigate human and financial losses while promoting sustainable watershed management.

Keywords: Flood Hazard Map; Frequency Storm, Hydraulic Modeling; Hydrological Modeling; Tireh Dorud River.

CITATION LINKS

[1] Pandit B., Bhattarai P.... [2] Shaikh A.A., Pathan A.I... [3] Ennouini W., Fenocchi A... [4] Bodoque J.M., Esteban-M... [5] Vashist K., Singh K.K. ... [6] Hojjati E, Talebi A, Da... [7] McDermott T.K. Global e... [8] Moshashaie S.M., Panahi... [9] Panahi R. Hosseinzadeh ... [10] Roostaei S., Eftekhar H... [11] Rahmati O., Darabi H., ... [12] Sami E. Ebadi M. Urban ... [13] Vafakhah M., Beigi H., ... [14] Ansori M.B., Lasminto U... [15] IOP. Conf. Ser. Earth. ... [16] Trinh M.X., Molkenthin ... [17] Farooq M., Shafique M.,... [18] Brunner G.W. HEC-RAS ri... [19] Siakara G., Gourgouleti... [20] Desalegn H., Mulu A. Ma... [21] Namara W.G., Damisse T.... [22] Hidayah E., Halik G., I... [23] Peker İ.B., Gülbaz S., ... [24] Ullah M.I., Qureshi K.S... [25] Sayyad D., Ghazavi R., ... [26] Moradi E., Ghanavati E.... [27] Esfandiari Darabad F., ... [28] Bai M., Tahmasebipour N... [29] Vafaei M., Dastoran, M.... [30] Vakili S., Erhami M., B... [31] Tahmasebi pour N., Dane... [32] Natarajan S., Radhakris... [33] US Army C.E., HEC-HMS U... [34] Chiang S., Chang C.H., ... [35] Hamdan A.N.A., Almuktar... [36] Verma R., Sharif M., Hu... [37] Ansari M.Z., Ahmad I., ... [38] Najafi Kalyani N, Ranjb... [39] Gunathilake M.B., Pandi... [40] Sepahvand T., Soleimani... [41] Guduru J.U., Mohammed A... [42] Hojjati E., Talebi A., ... [43] Maskey M.L., Nelson A.M... [44] Masteali S.H., Bayat M.... [45] Kulkarni A.D., Kale G.D... [46] Arash A.M., Yasi M. The... [47] Mokhtari D., Rezayi Mog... [48] Zeiger S.J., Hubbart J.... [49] Otmani A., Hazzab A., A... [50] Namazi Rad A., Mohseni ... [51] Janssen C. Manning's n ... [52] Te Chow V. Open channel... [53] Roostaei S., Mokhtari D... [54] Szopos N.M., Holb I.J.,... [55] Costabile P., Costanzo ... [56] Pinos J., Timbe L. Perf... [57] Plan and Budget Organiz... [58] Smith G.P., Davey E.K.,... [59] Iroume J.Y.A., Onguéné ... [60] Urzică A., Mihu-Pintili... [61] Prakash C., Ahirwar A.,... [62] Ranjan S., Singh V. HEC... [63] Liu T., McGuire L.A., Y... [64] Azevedo Toné A.J., Cunh... [65] Bindas T., Tsai W.P., L... [66] Duque L.F., O'Connell E... [67] Goswami G., Prasad R.K.... [68] Gervasi A.A., Pasternac... [69] Nederhoff K., Crosby, S... [70] Jamshidzade M., Bambeic... [71] Mirmousavi S.H., Taran ... [72] Vilca-Campana K., Carra...

Copyright© 2021, the Authors | Publishing Rights, ASPI. This open-access article is published under the terms of the Creative Commons Attribution-NonCommercial 4.0 International License which permits Share (copy and redistribute the material in any medium or format) and Adapt (remix, transform, and build upon the material) under the Attribution-NonCommercial terms.

Introduction

Flooding denotes the inundation of floodplains due to a river's channel capacity exceedance [1]. This hydrologic event can induce substantial socioeconomic and ecological impacts [2]. Floods, a natural hazard that is increasingly prevalent due to anthropogenic impacts on natural systems, cause substantial damage to urban infrastructure, socioeconomic services, and economic stability [3-6]. Studies indicate that 1.81 billion people (approximately 23% of the global population) are exposed to flood hazards and associated damages [7]. Iran has witnessed a series of catastrophic fluvial inundations in recent years. These events are not solely attributable to the exacerbating effects of climate change; anthropogenic factors stemming from suboptimal watershed management practices have played a significant role. Specifically, the expansion of urban and rural settlements, combined with unsustainable grazing pressures and deforestation, has resulted in a significant decline in the hydraulic conveyance capacity of riverine systems. Illustrative examples include the devastating floods of March and April 2019, which impacted 25 out of the nation's 31 provinces [8]. The provinces of Golestan, Ilam, Lorestan, and Khuzestan sustained particularly severe damage, resulting in over 77 fatalities and an estimated $2.2 billion in infrastructural losses across both urban and rural landscapes [9]. The escalating concentration of infrastructural development and socioeconomic capital within fluvial corridors and adjacent floodplains has amplified the exigency for robust flood assessment and estimation protocols to mitigate consequential impacts [10-11]. Given the heightened frequency of inundation events in recent decades and the inherent challenges in absolute prevention, implementing novel riparian zone management strategies and emphasizing flood resilience across diverse land-use and residential areas has become paramount [12-13]. While hydraulic structures play a role in flood control, comprehensive pluvial risk mitigation necessitates a robust geospatial database of inundation hazard mapping [8]. A fundamental aspect of effective flood hazard management involves delineating inundation-prone areas through hazard mapping to mitigate potential damage. However, this crucial step in developing nations often receives insufficient attention due to limitations in accessing high-resolution DEM (LiDAR) for accurate geospatial analysis [9,14]. Two primary methodologies exist for analyzing flood characteristics in River floodplains to assess hazards: the integration of Geographic Information Systems, remote sensing imagery, and historical records, and the application of numerical models for simulating riverine flow across these inundation zones. The latter approach is preferentially employed due to its enhanced capacity to scrutinize flood attributes and yield more precise prognostications [15]. Numerical flood models are categorized into one-dimensional (1D) and two-dimensional (2D) schematizations. While 1D models, such as SOBEK 1D, HEC-RAS 1D, and MIKE 1D, simplify flood propagation as unidirectional flow, neglecting lateral dynamics prevalent in real-world fluvial systems, 2D models account for flow in both longitudinal and transverse channel dimensions, rendering them more suitable for complex urban inundation scenarios [16]. Among numerical models employed in fluvial hydraulics, the Hydrologic Engineering Center's River Analysis System (HEC-RAS), developed by Brunner [17], stands as a prevalent tool for flood hazard simulation, adept at modeling steady and unsteady flow regimes, sediment transport, and temperature-dependent water quality assessments within watershed systems [18]. Numerous national and international

investigations have leveraged the HEC-RAS hydraulic model for River Flood hazard mapping within diverse watershed management paradigms. Selected pertinent research includes the study by Desalegn and Mulu, which utilized HEC-RAS and GIS for delineating flood zones in the Fetam River Watershed of Ethiopia. This research demonstrated that settlement areas and agricultural lands constitute significantly high-hazard zones across the entirety of the analyzed flood return periods [19]. In a study focusing on Ethiopia's upper Awash River watershed, Namara et al. employed integrated HEC-RAS and HEC-GeoRAS methodologies to generate flood inundation maps. Their findings indicated a progressive increase in the spatial extent of flooding, with inundated areas of 71.475, 76.630, 89.150, 100.290, 105.160, and 109.462 km^2 corresponding to 2-, 5-, 10-, 25-, 50-, and 100-year flood return intervals, respectively [20]. Hidayah et al.'s investigation, titled "Riverine Flood Hazard Mapping of the Pasuruan River in Indonesia Utilizing the HEC-RAS Model," elucidated that augmenting the flood recurrence interval from a biennial to a decennial scale engenders a discernible 37% escalation in the spatial extent of flood inundation within the delineated floodplain [21]. Peker et al.'s investigation into the Göksu River in Turkey, employing HEC-RAS and HEC-GeoRAS models for flood inundation mapping across varying return periods, identified a maximum flow depth of 10 meters and a peak flow velocity of 0.7 $m.s^{-1}$ within the fluvial reach under scrutiny [22]. Allah et al.'s investigation within the Swat River Watershed, employing the HEC-RAS hydraulic model, revealed that an increased flood recurrence interval is associated with a heightened fluvial inundation hazard within the study area [23]. Sayyad et al.'s research prepared a flood hazard map for the Suk-e-Cham River in Kashan, leveraging the HEC-RAS and RAS Mapper models. Their findings indicated that under a 100-year flood return period, approximately 41.5% and 4.5% of the Khancheh and Baronagh villages fall within the medium to very high flood risk classification [24]. Moradi et al.'s investigation generated a fluvial inundation map for the Kordan River within Alborz Province. Their research outcomes demonstrated that under return periods of 10, 25, 50, 100, 200, 500, and 1000 years, approximately 8, 17, 25, 32, 41, 53, and 64 hectares of residential, industrial, and fallow lands adjacent to the riverine corridor would be susceptible to flood encroachment [25]. In a hydrological assessment conducted by Esfandiari Darabad et al., employing the HEC-RAS model for morphological flood simulation in the Nooranchai River, Ardabil Province, the findings indicate that within a 200-year flood return period, approximately 329 hectares of urban and rural topographies are susceptible to inundation, potentially incurring substantial hydraulic losses [26]. Bay et al. developed a River Flood hazard map for the Qarachai Riverine reach in Golestan Province. Their research outcomes evinced that with augmented flood recurrence intervals across the watershed, the spatial extent, inundation depth, and concomitant flood risk escalate [27]. Vafaei et al. posited in their hydrographic investigation, "Flood Hazard Assessment of Ferdowsi University of Mashhad Campus Utilizing HEC-RAS and HEC-GeoRAS Models," that inundation events exceeding a 25-year recurrence interval at the terminal outfall of the campus and the Water and Electricity Canal Conduit precipitate deleterious impacts [28]. In a hydrologic investigation focusing on the delineation of a shrimp aquaculture site's inundation extent within Hormozgan Province, Vakili et al. ascertained that for a 100-year recurrence interval flood event, the peak discharge rates in designated drainage networks 1, 2, 3, 4, and 5 would be 86, 49, 60,

85, and 255 m^3. S^{-1}, respectively [29]. A review of the existing literature substantiates the robust performance of the Hydrologic Engineering Center's River Analysis System (HEC-RAS) in generating inundation maps and subsequently appraising flood risk. Consequently, the present research also employed the HEC-RAS model for flood hazard delineation and analysis. However, given that accurate flood hazard mapping and its subsequent rigorous analysis necessitate two-dimensional hydrodynamic modeling, an aspect underrepresented in prior investigations, this study utilized two-dimensional HEC-RAS modeling within the RAS Mapper environment to generate and analyze flood hazard maps for the Tireh Dorud River. This research aims to forecast flood hydrographs for recurrence intervals ranging from 2 to 500 years and analyze the two-dimensional flood hazard map by integrating inundation depth and flow velocity for the aforementioned return periods in the Tireh Dorud River within Lorestan Province.

Materials & Methods

Study Area

The urbanized area of Dorud, spanning 1,781 hectares, is the third most populous conurbation in Lorestan Province. It is geographically situated within the longitudinal range of 48° 58' 46" E to 49° 5' 45" E and has a latitudinal span of 33° 28' 38" N to 33° 32' 45" N (Figure 1). The city of Dorud, situated in a temperate mountainous climate, experiences the highest magnitude of precipitation within Lorestan province, with a mean annual rainfall of approximately 686 mm. Peak influxes are registered during the autumnal and early vernal months of October, November, December, and March, respectively. The Tireh Dorud River, the paramount fluvial system within Dorud City, extends for 11.314 km, with 3.716 km traversing the urban matrix. The residual segments are situated in the upstream and downstream reaches of Dorud. This riverine continuum constitutes a critical component of the Dez Watershed, ultimately discharging into the Persian Gulf [30]. Following the 2019 Dorud fluvial inundation event, a crisis management report identified infrastructural impairments affecting urban utilities, rural habitations, agricultural lands, and transportation arteries, which were quantified to have a fiscal burden exceeding 395.8769 billion Tomans.

Data Collection and Analysis

The present research aims to analyze a two-dimensional inundation hazard map for the Tireh Dorud River within Lorestan Province, considering return periods of 2, 5, 10, 20, 50, 100, 200, and 500 years. Consequently, to achieve the objectives mentioned above, hydrologic and hydraulic modeling were implemented utilizing HEC-HMS and HEC-RAS, respectively. Subsequently, inundation hazard maps corresponding to the specified recurrence intervals were generated and categorized within the RAS Mapper environment through the AIDR methodology. Figure 2 illustrates the flowchart of the research.

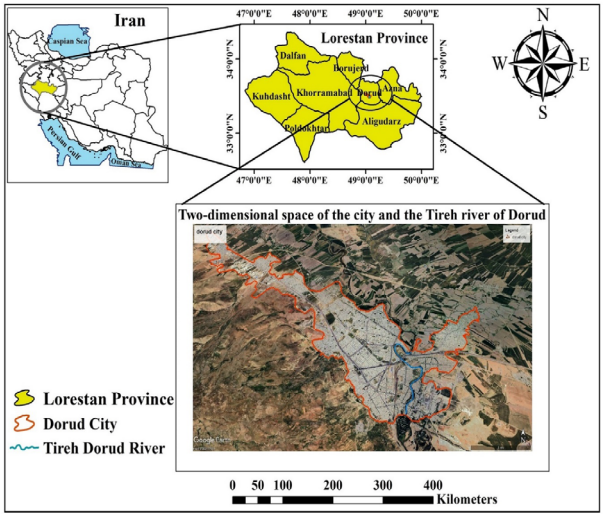

Figure 1) The location of the study area in Iran and Lorestan Province.

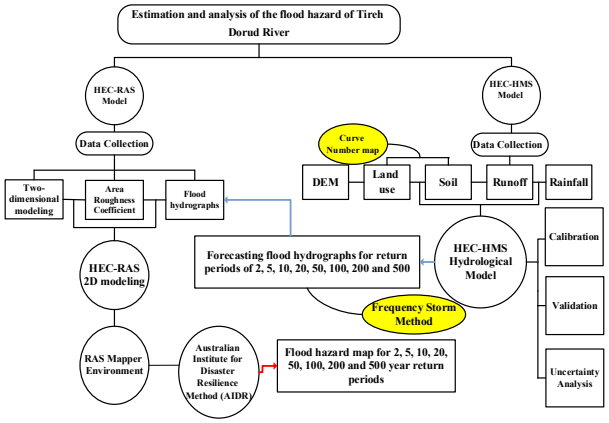

Figure 2) Flowchart for the research steps.

HEC-HMS Hydrological Modeling Generating Flood Hydrographs using HEC-HMS and Frequency Storm Methodology

The present investigation employed the Frequency Storm methodology [31], leveraging the HEC-HMS hydrologic model, to predict and evaluate flood hydrographs across various recurrence intervals (2, 5, 10, 20, 50, 100, 200, and 500 years). The Frequency Storm methodology generates a synthetic storm from statistical precipitation data. This method explicitly computes a hyetograph for each subbasin utilizing collected data. The Frequency Storm methodology features a Component Editor that holds parameter data for all subbasins within the Meteorological Model, along with distinct Component Editors for individual subbasins. The comprehensive Component Editor for the Meteorological Model encompasses parameter data detailing storm characteristics. This method is compatible with partial or annual-duration precipitation depth-duration data. When the computed flow output requires a different basis than the input precipitation, an Annual-Partial Ratio conversion factor can be applied. The Storm Duration dictates the precipitation event's length and must exceed the Intensity Duration. Regional historical storms can inform the selection of an appropriate Storm Duration. Conversely, the Intensity Duration defines the shortest storm period, typically aligning with the simulation time step, and must be less than the total storm duration. If the Simulation Duration surpasses the storm duration, subsequent time periods will register zero precipitation [32]. For this purpose, the requisite data for the HEC-HMS model, encompassing precipitation, discharge, DEM, soil, and Land-use, were initially procured. Notably, this investigation employed a DEM exhibiting a spatial resolution of 12.5 meters. At the same time, soil and land-use datasets were sourced from the Global Hydrologic Soil Groups website and the Esri 2020 Land-Cover database. Subsequently, the three constituents of the basin model, meteorological model, and control specifications were formulated for the designated area of inquiry [33]. In the present research, for the computation of basin model components, the Soil Conservation Service curve number method was employed for loss estimation, the unit hydrograph method for rainfall-runoff transformation, the recession method for baseflow separation, and the Muskingum method for flow routing [34-35]. For the derivation of the Curve Number map, 2022 Sentinel-2 land-use and hydrologic soil group maps were synergistically employed [36-37]. Subsequently, hyetograph methodologies and six-hour maximum precipitation data were used to quantify the meteorological component. Within the Control Specifications, simulation initialization and termination temporal parameters were input into the model, followed by model execution. Following the introduction of initial datasets into the model and the acquisition of preliminary outputs, the model calibration and validation phases were executed, consistent with prior investigations, utilizing two distinct events [38-39]. The model calibration and validation were implemented for the periods of February 24

to March 1, 2020, and March 24 to March 30, 2019, respectively, to mitigate possible errors and refine the modeling process. The performance metrics Percent Bias (PBIAS), Root Mean Square Error (RMSE), and Nash-Sutcliffe Efficiency (NSE) coefficient were employed for the comparative analysis of observed and simulated data within the hydrological modeling framework [40-41]. Flood hydrographs across recurrence intervals of 2, 5, 10, 20, 50, 100, 200, and 500 years were projected and estimated using the calibrated model in conjunction with the Frequency Storm methodology.

Parameter Uncertainty Estimation using Monte Carlo Methodology

The robustness and credibility of flood forecasts are contingent upon a comprehensive integration of all inherent sources of uncertainty within hydrological estimations. Among these, parametric uncertainty within hydrologic modeling frameworks is a primary driver of inaccuracies in flood hydrograph prediction [42]. This investigation employs a Monte Carlo simulation approach to rigorously characterize and propagate the uncertainty embedded within the predicted hydrograph. At its core, the Monte Carlo methodology involves the stochastic generation of plausible model realizations, derived from a probabilistic representation of uncertainty scenarios intrinsic to the watershed. Each uncertain input variable is iteratively sampled from its designated probability distribution function, enabling the computation of model outputs across an extensive ensemble of scenarios. This iterative procedure facilitates the examination of output variability and the sensitivity of model responses to parametric perturbations. A notable challenge within the Monte Carlo paradigm is the selection of appropriate probabilistic distributions for input variables. Due to data scarcity and the absence of comprehensive temporal records for specific parameters, a uniform distribution was used as a surrogate for the underlying probabilistic behavior [43]. The analysis specifically targeted the uncertainty quantification of three key hydrological parameters: The Curve Number (CN), the Recession coefficient, and the Muskingum routing coefficient.

HEC-RAS 2D Hydraulic Modeling Geometric Data Representation in RAS Mapper

In the present investigation, a 12.5-meter resolution DEM was obtained from ALOS PALSAR 12.5m DEM and utilized for delineating geometric data, Including Perimeter, Break lines, and boundary condition lines. The methodological approach involved delineating the two-dimensional floodplain and flow path within the RAS Mapper environment. Subsequently, based on the DEM, the demarcated floodplain and flow path were discretized into a computational mesh for hydrodynamic modeling, as depicted in Figure 3. The methodological approach involved delineating the Perimeters and Breaklines within the RAS Mapper environment. Subsequently, based on the DEM, the demarcated Perimeters and Breaklines were discretized into a computational mesh, as depicted in Figure 3, for hydrodynamic modeling [44]. It is pertinent to note that contemporary iterations of HEC-RAS incorporate an integrated module termed RAS Mapper, which endows the software with the intrinsic capacity for geometric data delineation, thereby obviating the necessity for the supplementary HEC-GeoRAS extension within the hydrodynamic modeling workflow [45]. Subsequently, upstream and downstream boundary conditions were defined. A flow hydrograph and normal depth were employed to ascertain these conditions for the upstream and downstream extents [46, 47].

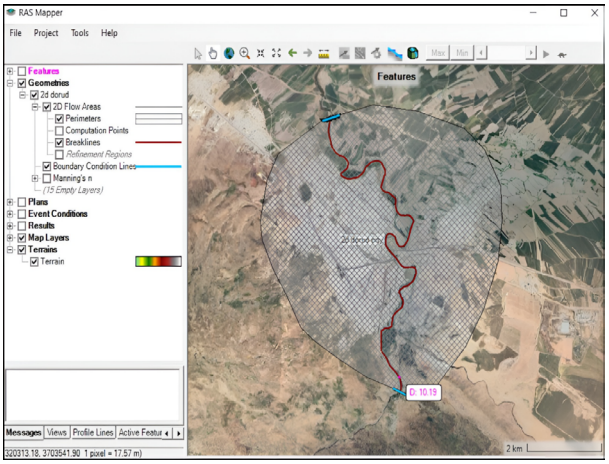

Figure 3) Geometric data (Perimeters, Breaklines, and Boundary Condition) structuring and 2D mesh generation within the RAS Mapper environment.

Manning's n Coefficient Estimation

A critical parameter in hydrodynamic modeling, Manning's roughness coefficient influences flow velocity and flood inundation extent within the fluvial system [8]. This coefficient quantifies the resistance exerted by the riverbed roughness and floodplain materials upon the flow path. Its magnitude can vary considerably depending upon factors encompassing hydraulic conditions, channel sinuosity, riverine geomorphology, bed material grain size distribution, as well as anthropogenic (Like creating obstacles in the flow path by humans) and natural (Vegetation) influences within the watershed context [9, 48-49]. Within this investigation, Manning's roughness coefficient map was generated by acquiring a 2020 land-cover map for the area of interest from the Esri database, derived from Sentinel-2 imagery. Subsequently, leveraging the generated land-use/land-cover map in conjunction with the Natural Resources Conservation Service (NRCS) methodology and Chow's suggested values (Figure 4), the spatial distribution of Manning's n was established [50-51], with resultant roughness coefficients for each land-cover category detailed in Table 1.

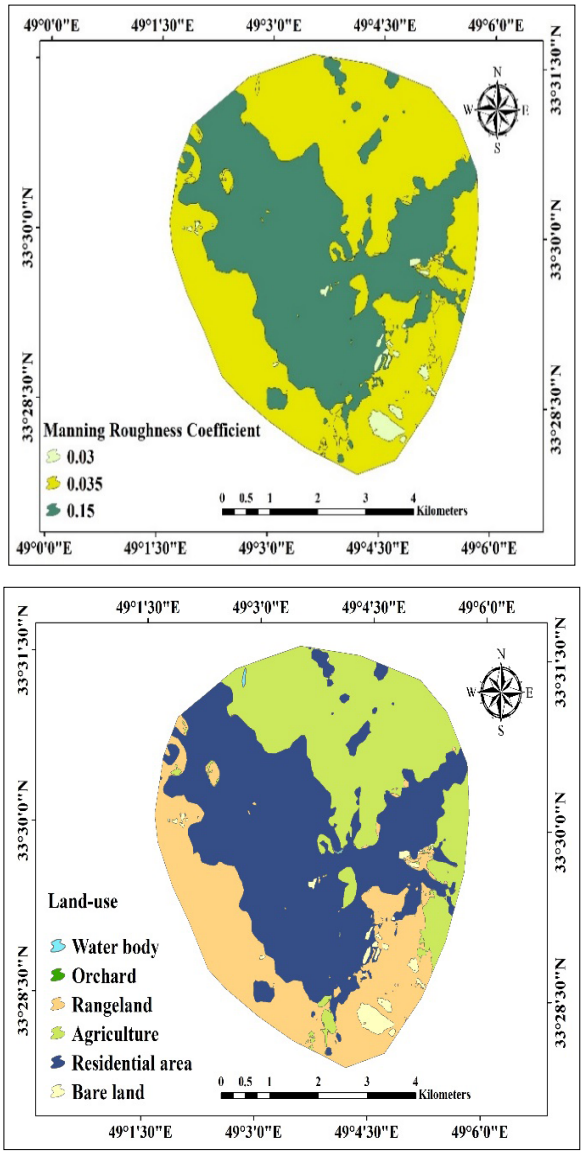

Figure 4) Land-use and Manning roughness coefficient maps in the study area.

Table 1) Land-use characteristics and Manning roughness coefficient of the study area.

Row	Land-use	Manning Roughness Coefficient
1	Water Body	0.035
2	Agriculture	0.035
3	Residential Area	0.15
4	Rangeland	0.035
5	Orchard	0.15
6	Bare land	0.03

2D HEC-RAS Hydraulic Modeling for AIDR-Based Inundation Hazard Mapping

The two-dimensional Hydraulic Engineering Center's River Analysis System (HEC-RAS) constitutes a prevalent computational hydraulics software developed by the US Army Corps of Engineers' Hydrologic Engineering Center [52]. This sophisticated tool enables users to perform analyses of unsteady and steady flow regimes for fluvial systems [53]. Leveraging physically based governing equations, this model provides a more realistic representation of the system, owing to the predominance of the horizontal dimension over the vertical [54,55]. While one-dimensional models exhibit efficacy in simulating in-channel processes, limitations arise upon overbank flow inundating the floodplain, necessitating higher-dimensional approaches for comprehensive flood hazard assessment [53]. In the present investigation, two-dimensional unsteady hydraulic modeling via HEC-RAS version 6.5 was employed to delineate flood inundation extents for various return periods. The numerical model was executed to compute flow depth and velocity for recurrence intervals of 2, 5, 10, 20, 50, 100, 200, and 500 years, subsequently generating flood hazard maps. Notably, flood hazard maps encompass various delineations, including flood inundation maps, flood depth and velocity variations, flood wave propagation velocity, and flood hazard zonation. Diverse methodologies exist for generating flood hazard maps across varying return periods. These encompass approaches employed by Australia (AIDR), NSW, FEMA, the Netherlands, and probabilistic flood inundation modeling [56]. Drawing upon propositions by researchers such as Smith et al. and Costabile et al., the Australian methodology (AIDR) demonstrates superior applicability for flood hazard categorization compared to the aforementioned approaches [54, 57]. Consequently, the Australian method (AIDR) was adopted in the present research for generating and classifying flood hazard maps. The AIDR methodology combines flow depth and velocity (depth × velocity) to generate and categorize flood hazard maps for various return periods. It ultimately classifies the flood hazard into six distinct categories (H1-H2-H3-H4-H5-H6) [24, 58, 59], as presented in Table 2. Ultimately, by implementing AIDR hazard classification algorithms within the RAS Mapper environment (Figure 5), flood hazard maps were derived across categories H1 to H6 for recurrence intervals of 2, 5, 10, 20, 50, 100, 200, and 500 years.

Table 2) AIDR table for hazard classification.

Flood Hazard	Hazard Level	Hazard Description
H1	No Flood Hazard	Generally safe for vehicles, people, and buildings
H2	Very Low Flood Hazard	Unsafe for small vehicles
H3	Low Flood Hazard	Unsafe for vehicles, children, and the elderly
H4	Moderate Flood Hazard	Unsafe for vehicles and people
H5	High Flood Hazard	Unsafe for vehicles and people. All the building types are vulnerable to structural damage. Some less robust building types are vulnerable to failure.
H6	Very High Flood Hazard	Unsafe for vehicles and people. All building types are considered vulnerable to failure.

Findings

Generation of Flood Hydrographs for Varying Recurrence Intervals

Within the scope of this investigation, the HEC-HMS model underwent sequential calibration and validation for the temporal windows spanning February 24, 2020, to

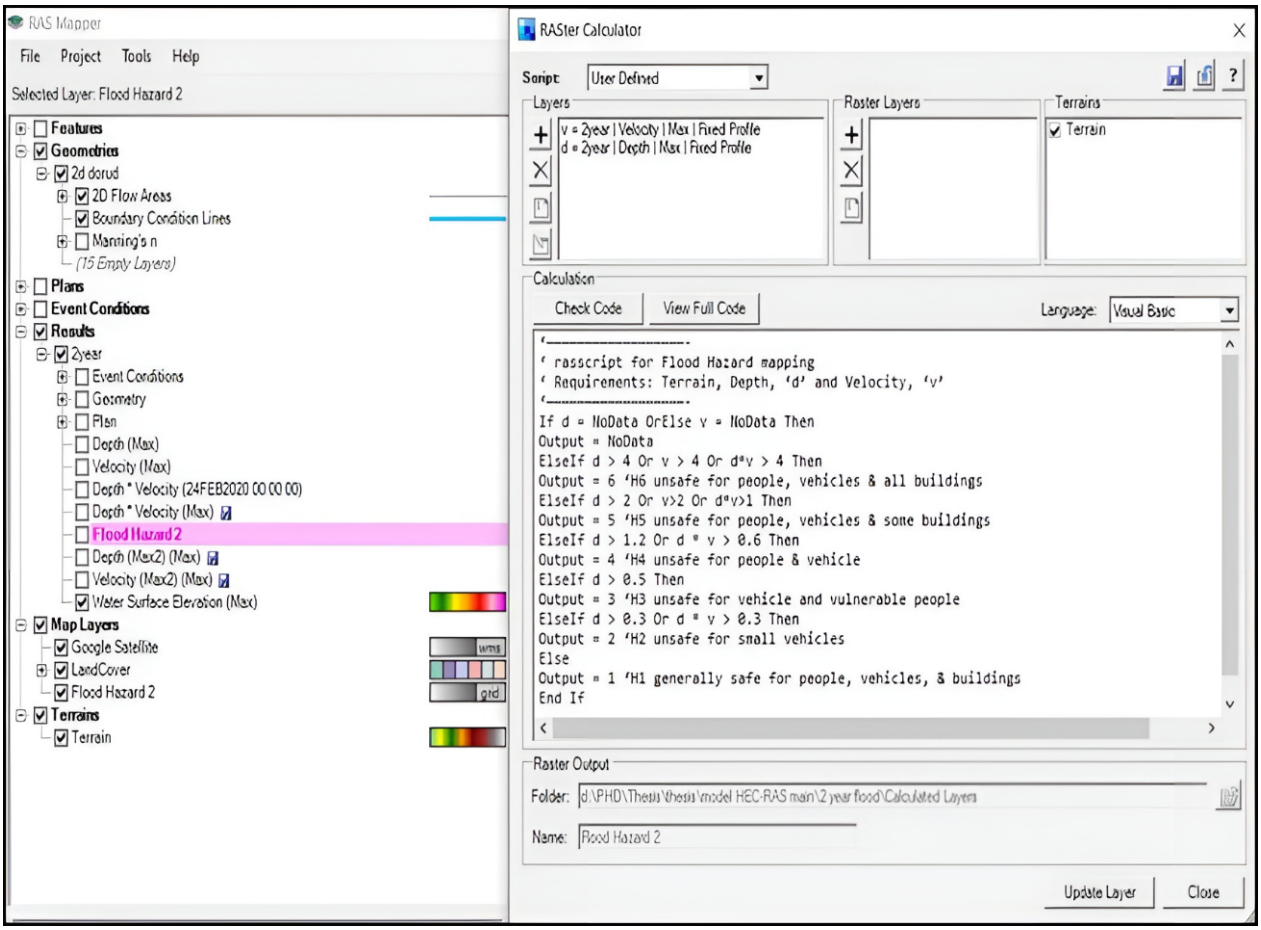

Figure 5) AIDR hazard classification algorithms within the RAS Mapper environment.

March 2, 2020, and March 24, 2019, to March 31, 2019, respectively. Figure 6 elucidates the observed and simulated hydrographs for the respective calibration and validation epochs. After calibration and validation of the model, the obtained statistical measures, including PBIAS, RMSE, and Nash-Sutcliffe efficiency coefficient, were 0.94, 0.2, and 0.969 for the calibration period and 14.15, 0.5, and 0.78 for the validation period, respectively. Table 3 presents the model performance metrics for the calibration and validation phases. After calibrating and validating the HEC-HMS model, employing the calibrated model structure and optimized parameter sets, flood hydrographs for recurrence intervals of 2, 5, 10, 20, 50, 100, 200, and 500 years were estimated utilizing the Frequency Storm methodology. Tabulated in Table 4 are the peak discharge estimations derived from the Frequency Storm methodology across varying recurrence intervals, revealing a discharge of 321.2 $m^3.s^{-1}$ for the 50-year event, 338.1 $m^3.s^{-1}$ for the 100-year event, 354.2 $m^3.s^{-1}$ for the 200-year event, and 373.5 $m^3.s^{-1}$ for the 500-year event.

Table 3) HEC-HMS model performance metrics for calibration and validation.

Stage	Calibration	Validation
Statistical Period	February 24th, 2020, to March 2nd, 2020	March 24th, 2019, to March 31st, 2019
PBIAS	0.94	14.15
RMSE	0.2	0.5
Nash-Sutcliffe	0.969	0.780

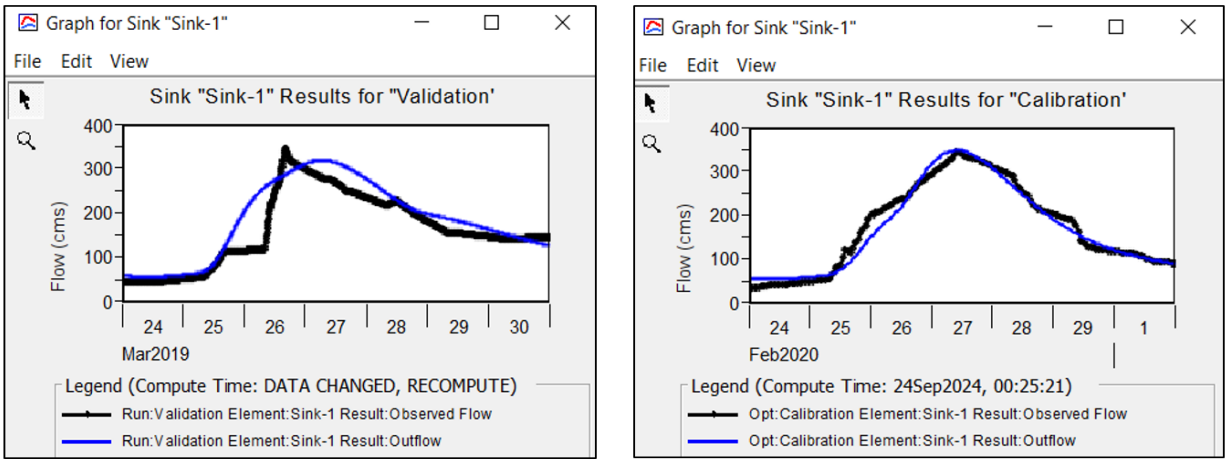

Figure 6) Hydrograph of observational and simulated data using the HEC-HMS Model.

Table 4) Peak discharge and Runoff depth estimation across varying recurrence intervals.

Return Period (Years)	Peak Discharge ($m^3.s^{-1}$)	Runoff Depth (mm)
2	210.2	70.43
5	254.2	82.48
10	278.0	88.98
20	298.1	94.44
50	321.2	100.78
100	338.1	105.37
200	354.2	109.80
500	376.5	115.89

Uncertainty Analysis of Parameter Variability in Flood Hydrograph Prediction

The Monte Carlo simulation technique was deployed to quantify the aggregate effect of all parameters influencing the uncertainty of the simulated flood hydrograph. A thousand iterative model realizations were performed, wherein each pertinent input parameter was systematically varied across its pre-defined range. Table 5 summarizes the statistical indicators of peak discharge uncertainty, delineating the contributions from the Curve Number (CN), Recession, and Muskingum routing coefficients. The results indicate that the CN, Recession, and Muskingum parameters contributed to peak discharge uncertainty at rates of approximately 0.72%, 2.10%, and 8.36%, respectively. These findings highlight the relative influence of key watershed response parameters on the robustness of hydrological predictions when accounting for parametric uncertainty.

Table 5) Statistical indicators of parameter uncertainty analysis in the peak discharge of the predicted flood hydrograph.

Statistical Criteria	Curve Number	Recession	Muskingum
Min	392.49	367.2	348.93
Max	448.40	524.87	1606.30
Mean	417.23	432.00	784.27
Standard Deviation	11.25	34.14	246.83
CV (%)	2.70	7.90	31.47
Uncertainty Range	55.91	157.64	1257.37
Uncertainty (%)	0.72	2.10	8.36

Flood inundation mapping in HEC-RAS and flood zone delineation

After geometric data (Perimeters, Breaklines, and Boundary Condition

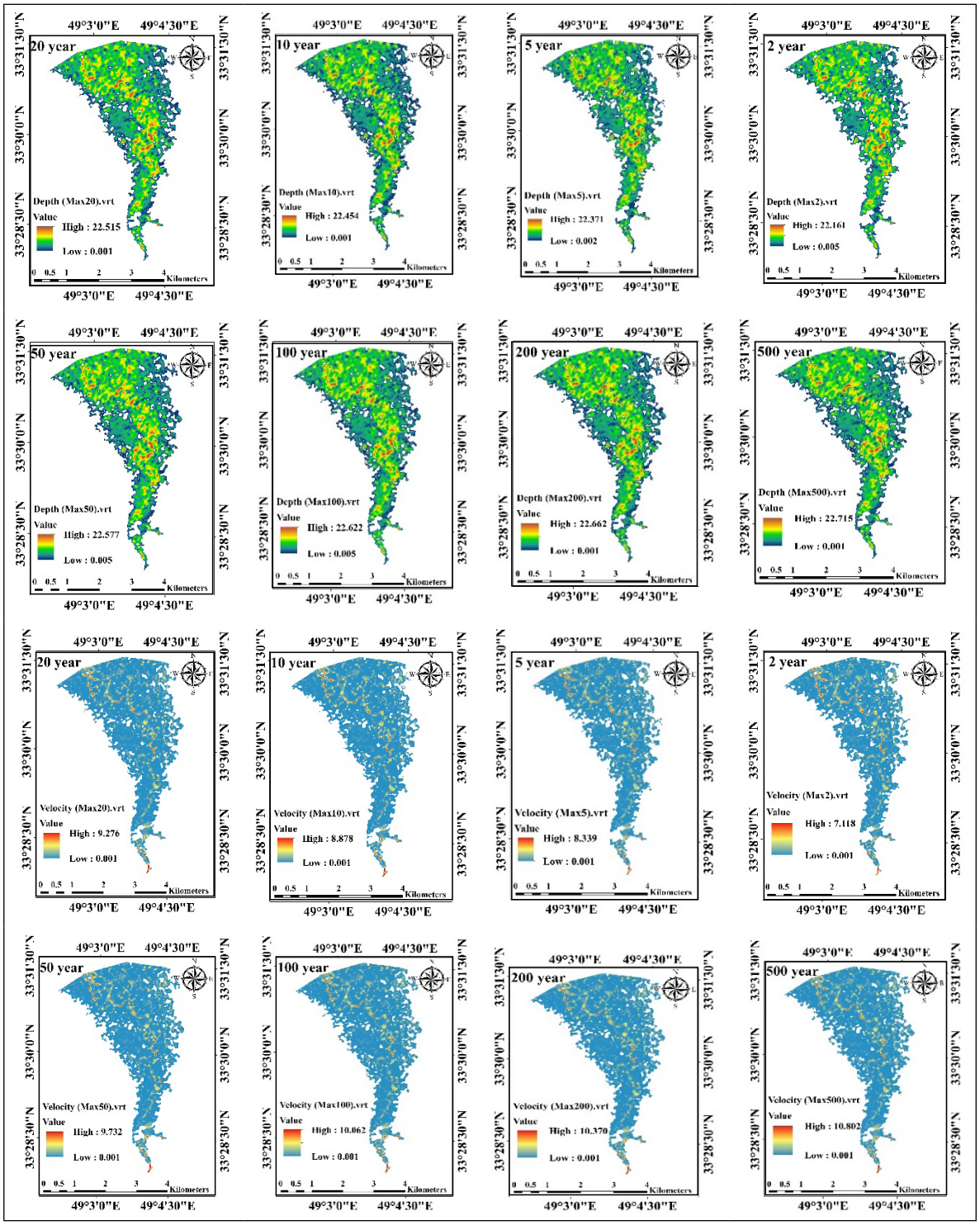

Figure 7) Flood inundation depth and velocity zonation across varying recurrence intervals.

Lines) delineation within the RAS Mapper environment and the incorporation of frequency Storm-derived flood hydrographs into the HEC-RAS model, flood inundation maps for 2, 5, 10, 20, 50, 100, 200, and 500-year recurrence intervals were generated. Corresponding flood depth and velocity maps were produced. Figure 7 illustrates the extent of flood depth and velocity across varying recurrence intervals. Table

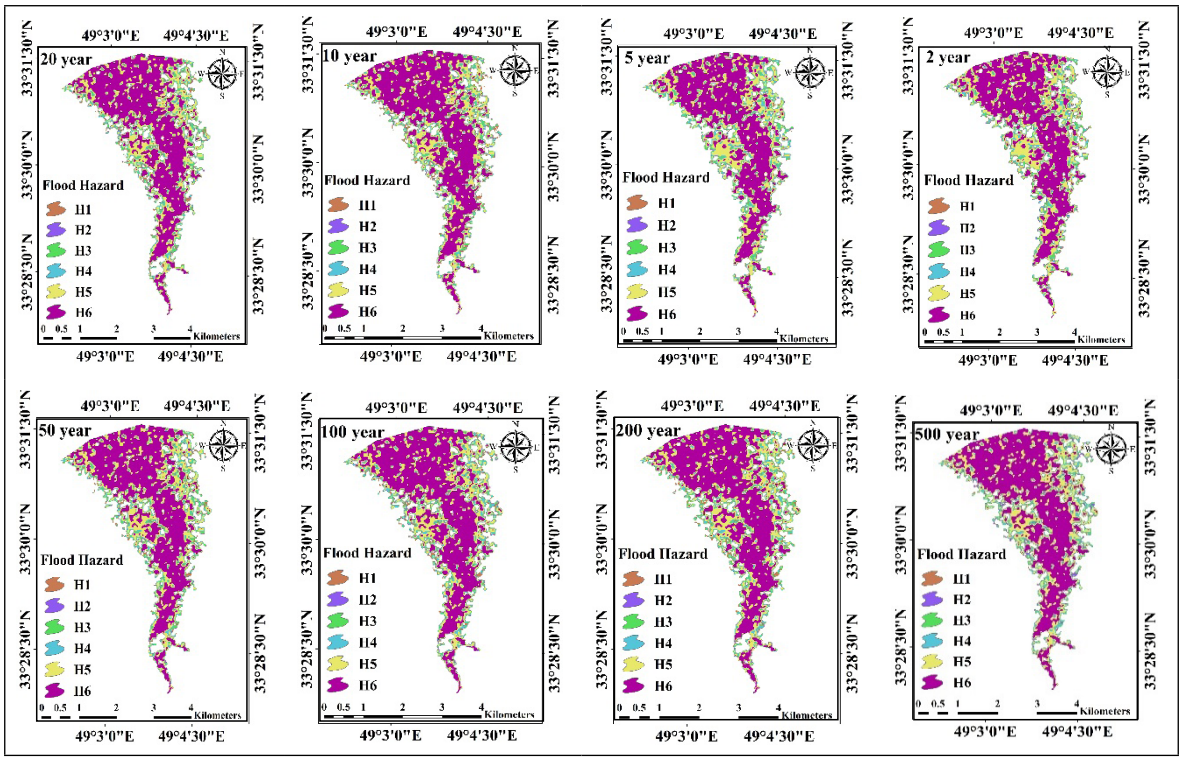

Figure 8) Generation of AIDR-based flood hazard maps within the RAS Mapper environment for recurrence intervals of 2, 5, 10, 20, 50, 100, 200, and 500 years.

6 presents the flood inundation area across varying recurrence intervals.

AIDR-Based Flood Hazard Zonation Generation Within the RAS Mapper Environment

Flood hazard maps for recurrence intervals of 2, 5, 10, 20, 50, 100, 200, and 500 years were delineated for the Tireh Dorud River in Dorud, leveraging the AIDR methodology and RAS Mapper scripting. This entailed utilizing HEC-RAS output maps of inundation depth and flow velocity. Subsequently, flood-prone areas were categorized into six distinct hazard classes: safe, very low hazard, low hazard, moderate hazard, high hazard, and very high hazard (H1, H2, H3, H4, H5, and H6) [3,54]. The resultant spatial distribution and quantitative attributes are presented in Figure 8 and Table 7, respectively. The findings reveal that across all analyzed recurrence intervals within the study area, the predominant flood hazard category corresponds to the very high hazard (H6). Specifically, the spatial extent classified as very high flood hazard constitutes 53.369%, 53.915%, 56.393%, 56.054%, 56.023%, 56.867%, 56.863%, and 57.305% of the total floodplain for the 2, 5, 10, 20, 50, 100, 200, and 500-year events, respectively.

Table 6) Areal extent of flood inundation across varying recurrence intervals.

Row	Flood Return Periods (Years)	Flood depth (km^2)
1	2	8.848
2	5	8.867
3	10	9.616
4	20	9.696
5	50	9.795
6	100	9.810
7	200	9.846
8	500	9.852

Table 7) AIDR-based flood hazard categorization across recurrence intervals of 2, 5, 10, 20, 50, 100, 200, and 500 years.

Return Period (Years)	Hazard Classification	Area (km²)	Area (%)
2	H1	0.244	2.689
	H2	0.157	1.726
	H3	0.551	6.068
	H4	0.779	8.584
	H5	2.502	27.564
	H6	4.845	53.369
5	H1	0.142	1.549
	H2	0.160	1.748
	H3	0.636	6.964
	H4	0.769	8.414
	H5	2.504	27.410
	H6	4.926	53.915
10	H1	0.338	3.597
	H2	0.171	1.818
	H3	0.561	5.978
	H4	0.660	7.039
	H5	2.362	25.175
	H6	5.292	56.393
20	H1	0.275	2.895
	H2	0.153	1.618
	H3	0.652	6.870
	H4	0.712	7.503
	H5	2.377	25.060
	H6	5.316	56.054
50	H1	0.280	2.921
	H2	0.146	1.522
	H3	0.688	7.178
	H4	0.700	7.303
	H5	2.402	25.053
	H6	5.371	56.023

Table 7 continued) AIDR-based flood hazard categorization across recurrence intervals of 2, 5, 10, 20, 50, 100, 200, and 500 years.

Return Period (Years)	Hazard Classification	Area (km^2)	Area (%)
100	H1	0.349	3.601
	H2	0.149	1.536
	H3	0.520	5.374
	H4	0.789	8.149
	H5	2.370	24.473
	H6	5.508	56.867
200	H1	0.336	3.462
	H2	0.090	0.922
	H3	0.593	6.111
	H4	0.791	8.150
	H5	2.378	24.492
	H6	5.520	56.863
500	H1	0.203	2.079
	H2	0.231	2.368
	H3	0.588	6.024
	H4	0.776	7.948
	H5	2.370	24.276
	H6	5.593	57.305

Discussion

Generation of Flood Hydrographs

According to the statistical criteria obtained, including PBIAS, RMSE, and Nash-Sutcliffe efficiency coefficient, the model demonstrates very good and good performance during the calibration and validation periods [60-61]. The peak discharge estimations derived from the Frequency Storm methodology across varying recurrence intervals demonstrate an escalating trend in peak discharge and runoff volume with increasing return periods, a finding congruent with the investigations of Namara et al [20]. The strong model performance, evinced by robust PBIAS, RMSE, and Nash-Sutcliffe coefficients, is crucial for reliable hydrological projections. This validates the escalating peak discharge trend with increasing return periods, mirroring recent studies on climate-driven extreme events [62]. Such congruence reinforces the model's predictive utility for flood hazard assessment. Uncertainty analysis revealed that the Muskingum coefficients demonstrate a greater degree of variability in comparison to the Curve Number and Recession coefficients. This heightened variability is likely a function of the intricate hydraulic interactions and dynamic geomorphic conditions prevalent across various channel segments. These factors are critical in governing the processes of flood routing, and their variability, in turn, disproportionately influences the

uncertainty surrounding peak discharge estimations throughout the watershed [63]. The outcomes of the Monte Carlo simulation unveil a pronounced divergence in the contributions of Muskingum and Curve Number (CN) parameters to peak discharge uncertainty. This phenomenon mirrors their distinct roles within the hydrological modeling paradigm. The CN coefficient, which epitomizes the surface characteristics and infiltration capacity of the watershed, accounted for a mere 0.72% of the total peak discharge uncertainty. This marginal contribution suggests that the model exhibits a low degree of sensitivity to fluctuations in this particular parameter. Such model stability can be attributed to the relatively homogeneous hydrological attributes of the study watershed, where CN variations fail to induce substantial changes in the overall watershed response. Consequently, this finding implies that a high level of precision in CN estimation may exert a lesser influence on the accuracy of peak discharge predictions when compared to other parameters. Conversely, the Muskingum routing coefficients were identified as the predominant source of uncertainty, contributing a significant 8.36%. This result corroborates the notion that the model is highly sensitive to changes in these parameters. The heightened sensitivity is defensible, as these coefficients directly govern the intricate processes of flood wave routing, including storage, translation, and attenuation, within the channel network. The hydrodynamic and geomorphic dynamics of stream channels, such as variations in slope, roughness, and cross-sectional geometry, exert a direct influence on these coefficients, causing any imprecision or uncertainty within them to be expeditiously reflected in the peak flow forecasts [64-65].

Flood Inundation Mapping in HEC-RAS

Based on the derived results, the spatial extent of flood depth and velocity exhibits a consistent pattern across all considered flood recurrence intervals, potentially attributable to the urban land-use characteristics of the region and its location within the floodplain [3]. Furthermore, the findings indicate a more extensive flood inundation in the upstream and midstream reaches of the study area, potentially stemming from the gentler slope gradient in the upper stream zone compared to the downstream section, coupled with the presence of alluvial plains in the upstream zone, a congruence observed in the research of Desalegn and Mulu [19]. The areal extent of flood inundation for recurrence intervals indicates a positive correlation between increasing return periods and the spatial expansion of flood-prone areas, a finding consistent with the research of Goswami et al. [66]. This observed constancy highlights how anthropogenic landscape modifications and inherent geomorphological attributes significantly influence hydraulic responses [3]. Notably, the role of urbanization in accelerating runoff and shaping flood propagation aligns with recent insights. The upstream inundation expansion, linked to gentler slopes and alluvial plains, reinforces principles of fluvial geomorphology, where topographic energy dictates flood extent. Slope inclination significantly impacts runoff generation and flood risk. Gentle slopes promote slower overland flow, allowing for increased soil saturation and water accumulation, which elevates flood levels and inundation duration. Conversely, steeper slopes facilitate rapid runoff, minimizing infiltration excess. Agricultural activities, such as intensive tillage, lead to soil compaction and reduced infiltration, while the removal of vegetative cover and wetlands diminishes the watershed's natural flood storage capacity. Effective floodplain management and soil conservation policies, including conservation tillage and

cover cropping, are crucial for mitigating downstream flood impacts by enhancing the watershed's hydrologic response. Moreover, the positive correlation between recurrence intervals and flood-prone areas emphasizes the non-linear increase in hazard footprints, necessitating adaptive hazard management strategies [67-68].

AIDR-Based Flood Hazard Zonation Generation

Based on the derived results, a greater spatial extent in the upstream reaches of the study area is susceptible to flood inundation, primarily due to the presence of agricultural lands. This phenomenon is attributed to the lower flow velocities across these cultivated areas, which leads to waterlogging and impedes timely floodwater recession [69]. Furthermore, in the central reaches of the study area, the presence of the Tireh Dorud River and subsequent overbank flooding during precipitation events have resulted in flood spillover beyond the channel conveyance. Consequently, local inhabitants have witnessed severe inundation episodes in the recent decade, notably the 2019 flood event, which substantially damaged urban infrastructure [70]. In March-April 2019, flooding in Dorud County caused significant damage, impacting 19 urban and 318 rural residential units, along with approximately 600 commercial and industrial establishments in Dorud City. Post-disaster assessments of affected areas like Dehno and Amirabad corroborate their classification within very high flood hazard zones, aligning with floodplain delineation studies. This analysis further reveals that agricultural land practices in upstream areas, characterized by reduced flow velocities, exacerbate waterlogging and prolong the duration of inundation. Such susceptibility aligns with recent research highlighting how agricultural modifications can intensify flood duration and impact local hydrology. The central reaches' vulnerability, tied to the Tireh Dorud River's overbank flooding and historical events like the 2019 flood, underscores the critical role of riverine geomorphology and extreme precipitation in urban flood resilience [71].

Conclusion

Inundation events, originating from extreme hydro-climatic natural processes that overwhelm the absorptive capacity of floodplains, lead to the significant perturbation of ecological systems and critical biotic zones due to their destructive impacts. This hazard represents a principal natural calamity within the Iranian territory, characterized by the recurrent annual manifestation of substantial flooding in at least one locale, resulting in considerable economic detriments and significant human casualties, with the potential for amplification through both inherent geomorphic factors (topography) and anthropogenic modifications (urbanization and agricultural practices). Given the occasional deliberate and un-engineered alterations to the riparian buffers and fluvial corridors traversing urbanized zones, contravening extant legal frameworks and technical specifications, the precise delineation of inundation characteristics and the extent of floodwater encroachment across varying recurrence intervals, a process termed flood zonation, assumes paramount significance for mitigating adverse flood impacts and formulating effective management strategies within high-hazard areas. The research findings indicate that, within this study, uncertainty arising from Muskingum routing parameters is demonstrably more critical than that associated with surface response parameters such as Curve Number (CN). This highlights the imperative of dedicating greater effort to the meticulous data collection and precise calibration of

flood routing parameters. Consequently, to enhance the accuracy of peak discharge forecasts, research endeavors and resources should be primarily directed toward refining the estimation of Muskingum coefficients over CN. This strategic focus will substantially improve modeling efficiency and facilitate more informed flood control management decisions. Based on the findings obtained within the upper and mid-reach segments of the delineated study area, a consequence of diminished gradient relative to the downstream sector is that the spatial extent of inundation is notably more expansive. Considering the prevalent land-use patterns in these zones, predominantly characterized by agricultural and residential activities, a substantial area remains susceptible to flood hazards across all analyzed recurrence intervals. Specifically, during the 2, 5, 10, 20, 50, 100, 200, and 500-year return periods, areas of 9.077, 9.137, 9.383, 9.484, 9.587, 9.685, 9.708, and 9.761 km^2, respectively, are projected to be at hazard of fluvial inundation. Furthermore, considering the derived outcomes across all recurrence intervals, a substantial proportion exceeding 50% of the flood-prone area is classified within the very high-hazard stratum, rendering these zones precarious for all structures, conveyances, and individuals. Urban morphology critically exacerbates flood risk by impeding natural hydrological processes. Channel constraints, resulting from urban development near waterways, reduce channel capacity and force overbank flow. Concurrently, high building density replaces permeable surfaces with impermeable surfaces, drastically increasing surface runoff and overwhelming urban drainage systems. This combination of reduced infiltration and constrained flow creates a feedback loop, thereby elevating flood hazards and underscoring why these areas consistently rank as "unsafe for all." This finding mandates the immediate prioritization of resources toward these zones, shifting the focus from non-structural measures to decisive structural interventions. Such engineering-based solutions, including the construction of levees, floodwalls, and retention basins, are essential for physical mitigation. Furthermore, the data necessitate a review of land-use policies to restrict development in high-risk areas and serve as a critical prompt for public preparedness and awareness. Consequently, it is recommended that the prevention of non-engineered construction within the riparian corridors and fluvial systems be prioritized, alongside the implementation of protective revetments and alternative flood control methodologies to avert infrastructure damage within the study perimeter. Addressing flood hazards effectively requires a dual approach, integrating non-structural and structural strategies to counteract the amplifying effects of urbanization and agriculture. Non-structural tactics involve rigorous floodplain zoning and land-use planning, prioritizing nature-based solutions like riparian buffer restoration and wetland creation to enhance natural flood attenuation, alongside promoting sustainable agricultural practices and developing robust early warning systems for community preparedness. Concurrently, structural interventions include targeted flood protection infrastructure (e.g., revetments, floodwalls), optimized urban drainage enhancements incorporating green infrastructure, and the establishment of controlled floodways. Ultimately, the success of these measures hinges on a collaborative Integrated Water Resource Management (IWRM) framework, tailoring solutions to specific geomorphological and anthropogenic contexts.

Limitations and Uncertainties of the Research

This study's findings are contextualized by

several inherent limitations and sources of uncertainty, primarily stemming from the modeling approach and the availability of data. The Monte Carlo simulation revealed that the Muskingum routing coefficients are the predominant source of uncertainty in the flood hydrograph generation, contributing a substantial 8.36% to the overall peak discharge variability. This highlights a fundamental limitation of the model's ability to fully capture the intricate hydrodynamic and geomorphic dynamics of the channel network. While the model simplifies these complex processes, its high sensitivity to Muskingum parameters underscores that model performance is highly contingent on the precision of these specific inputs. Conversely, the minimal contribution of the Curve Number (CN) (0.72%) suggests that the model is less sensitive to variations in surface-level parameters within the studied watershed. Furthermore, the accuracy of the flood inundation maps is directly tied to the resolution of the available Digital Elevation Model (DEM), which may not capture all intricate micro-topographical features that influence water flow.

Recommendation for Policy and Planning

The results of this research offer critical insights for effective flood hazard management and strategic planning. The identified vulnerability of the upstream and midstream reaches, primarily due to gentler slopes and prevalent agricultural and residential land-uses, mandates a review of existing land-use zoning policies. Policymakers should prioritize restricting development in these areas classified within the very high-hazard stratum. To enhance flood resilience, a dual approach integrating non-structural and structural interventions is recommended. Non-structural measures, such as riparian buffer restoration and the implementation of robust early warning systems, are essential for proactive mitigation. Concurrently, targeted structural interventions, including the construction of revetments and floodwalls, are necessary in high-risk zones, particularly along the Tireh Dorud River. Given the high sensitivity of the model to the Muskingum coefficients, future efforts should prioritize meticulous field surveys to obtain more accurate data for these parameters, thereby improving the reliability of peak discharge forecasts. Ultimately, these recommendations advocate for a comprehensive and Integrated Water Resource Management (IWRM) framework that tailors solutions to the specific geomorphological and anthropogenic context of the watershed.

Acknowledgments

The article's authors would like to express their sincere gratitude to the University of Kashan for their moral support in conducting the research.

Ethical permission: The authors certify that this manuscript is original and that any use of others' work or words has been appropriately cited.

Authors' Contributions: Z Naserian Asl: 50%- Software and statistical analysis, writing, and original draft preparation, manuscript editing, and **H Ghasemieh:** 50%- Supervision, conceptualization, manuscript review and editing, result control, manuscript editing.

Conflicts of Interests: This manuscript has not been published or presented elsewhere in part or in its entirety and is not under consideration by another journal.

Funding/Supports: This research did not receive specific funding from public, commercial, or not-for-profit agencies.

References

1. Pandit B., Bhattarai P. Flood risk mapping of Kamla River Basin using HEC-RAS 2D model. Int. J. Adv. Eng. Technol. 2023; 3(1): 31-45.
2. Shaikh A.A., Pathan A.I., Waikhom S.I., Agnihotri

P.G., Islam M.N., Singh S.K. Application of latest HEC-RAS version 6 for 2D hydrodynamic modeling through GIS framework: a case study from coastal urban floodplain in India. Model Earth. Syst. Environ. 2023; 9(1): 1369-1385.
3. Ennouini W., Fenocchi A., Petaccia G., Persi E., Sibilla S.A., complete methodology to assess hydraulic risk in small ungauged catchments based on HEC-RAS 2D Rain-On-Grid simulations. Nat. Hazards. 2024; 120(8): 7381-7409.
4. Bodoque J.M., Esteban-Muñoz Á., Ballesteros-Cánovas J.A. Overlooking probabilistic mapping renders urban flood risk management inequitable. Commun. Earth. Environ. 2023; 4(1): 279.
5. Vashist K., Singh K.K. EC-RAS 2D modeling for flood inundation mapping: a case study of the Krishna River Basin. Water. Pract. Technol. 2023; 18(4): 831-844.
6. Hojjati E, Talebi A, Dastorani M T, Salaghegeh A. Developing a distributed hydrological balance model for predicting runoff in urban areas in Tehran, the Capital of Iran. ECOPERSIA 2024; 12 (2):93-109.
7. McDermott T.K. Global exposure to flood risk and poverty. Nat. Commun. 2022; 13(1): 3529.
8. Moshashaie S.M., Panahi R., Moshashaie M. Dynamic Analysis of Flood Risk using HEC-RAS Hydraulic Model (Case Study: Shahinshahr River, Isfahan Province). J. Geo. Environ. Hazards. 2022; 11(1): 77-97.
9. Panahi R. Hosseinzadeh M.M. Zoning and morphological analysis of floods of Dinevar River (Kermanshah province) using the HEC-RAS hydrodynamic model. J. Geo. Environ. Hazards. 2021; 9(4): 45-64.
10. Roostaei S., Eftekhar H., Karami F., Neghaban S. Garlic cybernetics urban watershed basins flood coefficient using the normal distribution model (Case study: Watershed of Shiraz). Quant. Geomorphol. Res. 2022; 11(3): 23-38.
11. Rahmati O., Darabi H., Haghighi A.T., Stefanidis S., Kornejady A., Nalivan O.A., Tien Bui D. Urban flood hazard modeling using self-organizing map neural network. Water 2019; 11(11): 2370.
12. Sami E. Ebadi M. Urban flood hazard zoning using fuzzy-analytic network process (ANP), Case study: Maragheh City. J. Urb Eco. Res. 2024; 15(1): 171-186.
13. Vafakhah M., Beigi H., Sadeghian K., Khodamoradi H., Karimi Breshneh S., Daeichini F. Flood peak discharge trend over Iran. ECOPERSIA 2024; 12 (3): 219-231.
14. Ansori M.B., Lasminto U., Kartika A.A.G. Reliability of runoff hydrograph model for extreme rainfall events using HEC-RAS 2D Flow Hydrodynamics Rain-On-Grid.
15. IOP. Conf. Ser. Earth. Environ. Sci. 2023; 1276(1): p. 012034.
16. Trinh M.X., Molkenthin F. Flood hazard mapping for data-scarce and ungauged coastal river basins using advanced hydrodynamic models, high temporal-spatial resolution remote sensing precipitation data, and satellite imageries. Nat. Hazard. 2021; 109(1): 441-469.
17. Farooq M., Shafique M., Khattak M.S. Flood hazard assessment and mapping of River Swat using HEC-RAS 2D model and high-resolution 12-m TanDEM-X DEM (WorldDEM). Nat. Hazards. 2019; 97(1): 477-492.
18. Brunner G.W. HEC-RAS river analysis system: User's manual. US Army Corps of Engineers, Institute for Water Resources, Hydrologic Engineering Center. 2002.
19. Siakara G., Gourgouletis N., Baltas E. Assessing the efficiency of fully two-dimensional hydraulic HEC-RAS Models in rivers of Cyprus. Geographies 2024; 4(3): 513-536.
20. Desalegn H., Mulu A. Mapping flood inundation areas using GIS and HEC-RAS model at Fetam River, Upper Abbay Basin, Ethiopia. Sci. Afr. 2021; 12: e00834.
21. Namara W.G., Damisse T.A., Tufa F.G. Application of HEC-RAS and HEC-GeoRAS model for flood inundation mapping, the case of Awash Bello Flood plain, upper Awash River Basin, Oromiya Regional State, Ethiopia. Model Earth Syst. Environ. 2022; 8(2): 1449-1460.
22. Hidayah E., Halik G., Indarto I., Khaulan D.W. Flood hazard mapping of the Welang River, Pasuruan, East Java, Indonesia. J. App. Wat. Eng. Res. 2023; 11(3): 333-344.
23. Peker İ.B., Gülbaz S., Demir V., Orhan O., Beden N. Integration of HEC-RAS and HEC-HMS with GIS in flood modeling and flood hazard mapping. Sustainability 2024; 16(3): 1226.
24. Ullah M.I., Qureshi K.S., Rauf A.U., Shah L.A. Advanced floodplain mapping: HEC-RAS and ArcGIS Pro application on the Swat River. J. of Umm Al-Qura Uni. Eng. Arc. 2024; 15(3): 245-258.
25. Sayyad D., Ghazavi R., Omidvar E. Preparation and analysis of flood risk map using HEC RAS and RAS MAPPER hydraulic model (Case study: Sok Cham river of Kashan). J. Geo. Environ. Hazards. 2021; 10(3): 19-37.
26. Moradi E., Ghanavati E., Ahmadabadi A., Saffary A. The role of human factors in geomorphic imbalances of the Kordan River using satellite images and HEC-RAS software. Quant. Geomorphol. Res. 2022; 11(2): 150-168.
27. Esfandiari Darabad F., Nezafat Taklreh B., Paseban A.H. Morphological Simulation of Flood Occurrence in Nooranchai River Using HEC-RAS

Hydraulic Model. Environ. Erosion Res. J. 2022; 12(3): 190-210.
28. Bai M., Tahmasebipour N., Zeinivand H., Sadoddin A., Kaheh M. Investigating the two-dimensional HEC-RAS Model capability for flood risk mapping in the Qarachai River in Ramian, Golestan Province. Geogr. Environ. Hazards. 2024; 12(4): 187-203.
29. Vafaei M., Dastoran, M.T. Rostami Khalaj M. Flood risk assessment in the campus of Ferdowsi University of Mashhad and presentation management scenarios using the HEC-RAS model. Water Soil Manage. Model. 2022; 3(3): 225-239.
30. Vakili S., Erhami M., Baghdadi H. Organization of Lashtaghan shrimp breeding site with HEC-RAS two-dimensional model. Watershed Eng. Manage. 2024; 16(2): 185-200.
31. Tahmasebi pour N., Daneshfar M. Beyranvand, K. Evaluation of the efficiency of experimental methods for estimating design discharge in the Tireh Dorud Basin. 11th National Conference on Watershed Management Science and Engineering of Iran. 2016.
32. Natarajan S., Radhakrishnan N. Simulation of extreme event-based rainfall–runoff process of an urban catchment area using HEC-HMS. Model Earth Syst. Environ. 2019; 5(4): 1867-1881.
33. US Army C.E., HEC-HMS User's Manual 2016.
34. Chiang S., Chang C.H., Chen W.B. Comparison of rainfall-runoff simulation between support vector regression and HEC-HMS for a rural watershed in Taiwan. Water 2022; 14(2): 191.
35. Hamdan A.N.A., Almuktar S., Scholz M. Rainfall-runoff modeling using the HEC-HMS model for the Al-Adhaim river catchment, northern Iraq. Hydrology 2021; 8(2): 58.
36. Verma R., Sharif M., Husain A. Application of HEC-HMS for hydrological modeling of upper Sabarmati River Basin, Gujarat, India. Model Earth Syst. Environ. 2022; 8(4): 5585-5593.
37. Ansari M.Z., Ahmad I., Rautela K.S., Goyal M.K., Singh P.K. Hydrological modelling using HEC-HMS and estimation of the flood peak by Gumbel's Method. Sus. Res. Dev. 2023; 173-190.
38. Najafi Kalyani N, Ranjbar-Fordoei A, Fatemeh P, Musavi H. Prediction of soil hydrological responses under land use/cover changes using Markov Chains in Jiroft Watershed, Iran. ECOPERSIA 2022; 10(1):47-59.
39. Gunathilake M.B., Panditharathne P., Gunathilake A.S., Warakagoda N.D. Application of a HEC-HMS model on event-based simulations in a tropical watershed. Eng. App. Sci. Res. 2020; 47(4): 349-360.
40. Sepahvand T., Soleimani- Motlagh M., Zeinivand H., Mirzaei Mosivand A. Estimating Flood through the Fractal Theory-Based Precipitation Estimation and the CN Extracted from Sentinel 2 in HEC-HMS Model: A Case Study of Thireh Watershed in Borujerd-Dorud Region. Des. Eco. Eng. 2023; 12(38): 87-103.
41. Guduru J.U., Mohammed A.S. Hydrological Modeling Using HEC-HMS Model, Case of Tikur Wuha River Basin, Rift Valley River Basin, Ethiopia. Environ. Chall. 2024; 17: 101017.
42. Hojjati E., Talebi A., Dastorani M.T., Salaghegeh A. Developing a distributed hydrological balance model for predicting runoff in urban areas in Tehran, the Capital of Iran. ECOPERSIA 2024; 12 (2):93-109.
43. Maskey M.L., Nelson A.M., Moriasi D.N., Northup B.K. Uncertainty analysis of hydrological parameters of the APEXgraze model for grazing activities. Ecol. Model. 2025; 499: 110917.
44. Masteali S.H., Bayat M., Bettinger P., Ghorbanpour M. Uncertainty analysis of linear and non-linear regression models in the modeling of water quality in the Caspian Sea basin: Application of Monte-Carlo method. Ecol. Indic. 2025; 170:112979.
45. Kulkarni A.D., Kale G.D. The Development of Coupled 1D–2D Hydrodynamic flood model by using HEC-RAS: A case study of the Panchganga River Basin, Kolhapur District, Maharashtra, India. Wat. Res. 2024; 51(5): 789-799.
46. Arash A.M., Yasi M. The assessment for selection and correction of RS-based DEMs and 1D and 2D HEC-RAS models for flood mapping in different river types. J. Flood Risk Manag. 2023; 16(1): e12871.
47. Mokhtari D., Rezayi Moghadam M.H., Moazzez S. Dynamic Analysis of Flood Hazard in Active Alluvial fan using the HEC-RAS Hydrodynamic Model and GIS Technique (Case Study: Leilan Alluvial fans, Northwest of Iran). Quan. Geo. Res. 2021; 9(4): 169-185.
48. Zeiger S.J., Hubbart J.A. Measuring and modeling event-based environmental flows: An assessment of HEC-RAS 2D rain-on-grid simulations. J. Environ. Manage. 2021; 285: 112125.
49. Otmani A., Hazzab A., Atallah M. H., Apollonio C., Petroselli A. Using volunteered geographic information data for flood mapping–Wadi Deffa El Bayadh, Algeria. J. App. Wat. Eng. Res. 2023; 11(4): 464-480.
50. Namazi Rad A., Mohseni N., Hosseinzadeh S.R. Flood inundation monitoring using Sentinel SAR data and hydraulic modeling. Quan. Geo. Res. 2021; 10(3): 40-56.
51. Janssen C. Manning's n values for various land covers to use for dam breach analyses by NRCS in Kansas. Revised by PAC. 2016.
52. Te Chow V. Open channel hydraulics. 1959.

53. Roostaei S., Mokhtari D., Faraji A., Flood simulation on compaction forms by geomorphological indices and HEC-RAS hydraulic model (Case study of Pardisan Town, Qom). Quan. Geo. Res. 2023; 12(1): 40-58.
54. Szopos N.M., Holb I.J., Dávid A., Szabó S. Flood risk assessment of a small river with limited available data. Spa. Inf. Res. 2024; 32(6): 787-800.
55. Costabile P., Costanzo C., Ferraro D., Macchione F., Petaccia G. Performances of the new HEC-RAS version 5 for 2-D hydrodynamic-based rainfall-runoff simulations at basin scale: Comparison with a state-of-the-art model. Water 2020; 12(9): 2326.
56. Pinos J., Timbe L. Performance assessment of two-dimensional hydraulic models for generation of flood inundation maps in mountain river basins. Wat. Sci. Eng. 2019; 12(1):11-18.
57. Plan and Budget Organization. Manual for Providing Flood Risk Map. 2020; No. 821.
58. Smith G.P., Davey E.K., Cox R.J., Flood hazard. Technical report 2014/07, Water Research Laboratory, University of New South Wales, Sydney. 2014.
59. Iroume J.Y.A., Onguéné R., Djanna Koffi F., Colmet-Daage A., Stieglitz T., Essoh Sone W., Etame J. The August 21, 2020, flood in Douala (Cameroon): A major urban flood investigated with 2D HEC-RAS modeling. Water 2022; 14(11): 1768.
60. Urzică A., Mihu-Pintilie A., Stoleriu C.C., Cîmpianu C.I., Huţanu E., Pricop C.I., Grozavu A. Using 2D HEC-RAS modeling and embankment dam break scenario for assessing the flood control capacity of a multi-reservoir system (NE Romania). Water 2021; 13(1): 57.
61. Prakash C., Ahirwar A., Lohani A.K., Singh H.P. Comparative analysis of HEC-HMS and SWAT hydrological models for simulating the streamflow in a sub-humid tropical region in India. Environ. Sci. Pollut. Res. Int. 2024; 31(28): 41182-41196.
62. Ranjan S., Singh V. HEC-HMS-based rainfall-runoff model for Punpun River Basin. Water Pract. Technol. 2022; 17(5): 986-1001.
63. Liu T., McGuire L.A., Youberg A.M., Abolt C.J., Atchley A.L. Temporal persistence of postfire flood hazards under present and future climate conditions in southern Arizona, USA. NHESSD. 2024; 1-27.
64. Azevedo Toné A.J., Cunha Costa A., Ubirajara G. Barros M., Lima Neto I.E. Streamflow prediction based on data-scarce river-aquifer dynamics estimated by a simplified modelling framework in a dryland catchment. MESE. 2025; 11(4): 282.
65. Bindas T., Tsai W.P., Liu J., Rahmani F., Feng D., Bian Y., Shen C. Improving river routing using a differentiable Muskingum-Cunge model and physics-informed machine learning. Water Resour. Res. 2024; 60(1): e2023WR035337.
66. Duque L.F., O'Connell E., O'Donnell G.A. Monte Carlo simulation and sensitivity analysis framework demonstrating the advantages of probabilistic forecasting over deterministic forecasting in terms of flood warning reliability. J. Hydrol. 2023; 619, 129340.
67. Goswami G., Prasad R.K., Kumar D. Hydrodynamic flood modeling of Dikrong River in Arunachal Pradesh, India: a simplified approach using HEC-RAS 6.1. Model Earth Syst. Environ. 2023; 9(1): 331-345.
68. Gervasi A.A., Pasternack G.B., East A.E. Flooding duration and volume more important than peak discharge in explaining 18 years of gravel–cobble river change. Earth Surf. Process. Landforms. 2021; 46(15): 3194-3212.
69. Nederhoff K., Crosby, S.C., Van Arendonk N.R., Grossman E. E., Tehranirad B., Leijnse, T., Barnard, P.L. Dynamic modeling of coastal compound flooding hazards due to tides, extratropical storms, waves, and sea-level rise: a case study in the Salish Sea, Washington (USA). Water, 2024; 16(2): 346.
70. Jamshidzade M., Bambeichi S., Parvaresh Rizi A., Flood Hazard and Vulnerability Analysis at Drainage Networks, Case Study of Shuaibieh Plain. Water Irr. Manage. 2023; 13(4): 1035-1052.
71. Mirmousavi S.H., Taran Z. Monitoring and detection of Lorestan 2019 flood using satellite data in Google Earth Engine. App. Geo. information sys. Rem. Sen. in planning. 2023; 2(14): 7-18.
72. Vilca-Campana K., Carrasco-Valencia L., Iruri-Ramos C., Cárdenas-Pillco B., Escudero A., Chanove-Manrique A. Improving Urban Flood Resilience: Urban Flood Risk Mitigation Assessment Using a Geospatial Model in the Urban Section of a River Corridor. Water, 2025; 17(7): 1047.